High-Precision EMG Signal Decomposition Using Communication Techniques

Richard Gut, *Member, IEEE*, and George S. Moschytz, *Fellow, IEEE*

***Abstract*—This paper presents a new approach to the decomposition of *electromyographic* (EMG) signals. EMG signals consist of a superposition of delayed finite-duration waveforms that carry the information about the firing of different muscle fiber groups. The new approach is based on a communication technical interpretation of the EMG signal. The source is modeled as a signaling system with intersymbol-interference, which encodes a well-defined sparse information sequence. This point of view allows a *maximum-likelihood* (ML) as well as a *maximum a posteriori* (MAP) estimation of the underlying firing pattern to be made. The high accuracy attainable with the proposed method is illustrated both with measured and artificially generated EMG signals.**

***Index Terms*—Digital communication, digital signal processing, electromyography.**

I. Introduction

AN electromyographic (EMG) SIGNAL is generally obtained by measuring the electrical activity in a muscle using a needle electrode. The observed signal represents the depolarization of the muscle fiber membranes which create an electrical signal. An individual motor neuron and its corresponding muscle fibers are referred to as a *motor unit* (MU). The waveform produced by such a muscle fiber group is called a *motor unit action potential* (MUAP). The shape of a MUAP depends on the geometry of the needle electrode, its position relative to the fiber group, and the MU itself. The shape is, furthermore, a function of muscle force, muscle fatigue, and of the age of the patient. A disease of the peripheral nervous system results in a change of the characteristics of the MUAPs. The time domain representation of the MUAPs, i.e., the duration as well as the number of phases have proven to be a useful clinical diagnostic tool in the evaluation of patients with neuropathies and myopathies [1]–[3]. The number of active MUs and their firing rates are controlled by the central nervous system in accordance with the muscle force produced. Up to about ten MUs can be observed using a conventional coaxial needle electrode. The complete firing pattern (the so-called innervation pattern) and the corresponding statistics of the MUs involved are mainly used for investigations of the neuromuscular control loop. Up until the late 1970s, manual decomposition of the EMG signal was used. However, manual analysis is quite tedious and time consuming. During the early 1980s, investigators began automating this process [4]–[9]. In the last few years, several neural-network-based algorithms have been published. See an excellent review of current and past activities in EMG research in [10]. Although extraordinary progress has been made in this field, the problem is still not considered completely solved. The algorithms published until now are mainly designed to extract the MUAP's from the EMG signal and do not aim at finding the precise innervation pattern. Even at a moderate muscle force, the achievement of 90% or more correct estimated innervations still requires the use of an expensive, custom-designed multichannel electrode [4], [11] or special collection techniques.

The primary goal of this paper is to show how established communication techniques can be beneficially exploited in fields well beyond those of communications as, in our case, that of EMG signal decomposition. Since the decomposition of EMG signals is a typical problem in signal processing, we believe that our method of analysis could be applied also to other signals such as ECGs. A modified version of the basic concept has already been successfully used in the field of nondestructive testing [12] and could be applied also to medical ultrasonic-imaging systems [13]. In fact, we wish to point out that the new concept can theoretically be generalized to perform a joint estimation [14] of the shape of MUAP's and their innervation sequence hidden in the EMG signal. A practical realization would certainly have a strong impact on other fields since the EMG signal is referred to as a key example of a class of signals that can be interpreted only by a multistage approach [10]. The joint estimation would solve the problem in a single step.

This paper is organized as follows. Section II briefly covers the background of the EMG analysis and shows how the *a priori* unknown MUAPs are determined. In Section III, the mathematical model, which is normally used for EMG signals, is developed into a signaling system with intersymbol interference. Section IV is the backbone of this paper and presents the MAP innervation sequence estimation in detail. Results obtained with the ML and MAP estimation schemes, and for measured and artificially generated EMG's, are given in Section V. Section VI concludes the paper. Preliminary results and the basic concept of the ML estimation scheme were reported in [15].

II. Analysis of the EMG Signal

EMG analysis is generally subdivided into two main phases (Fig. 1). The first is a data preprocessing phase, in which the

Manuscript received April 7, 1997; revised April 19, 2000. The associate editor coordinating the review of this paper and approving it for publication was Dr. Sergios Theodoridis.

R. Gut is with the University of Applied Scienies, Muttenz, Switzerland (e-mail: r.gut@fhbb.ch).

G. S. Moschytz is with the Institute for Signal and Information Processing, Swiss Federal Institute of Technology, Zürich, Switzerland.

Publisher Item Identifier S 1053-587X(00)06686-1.

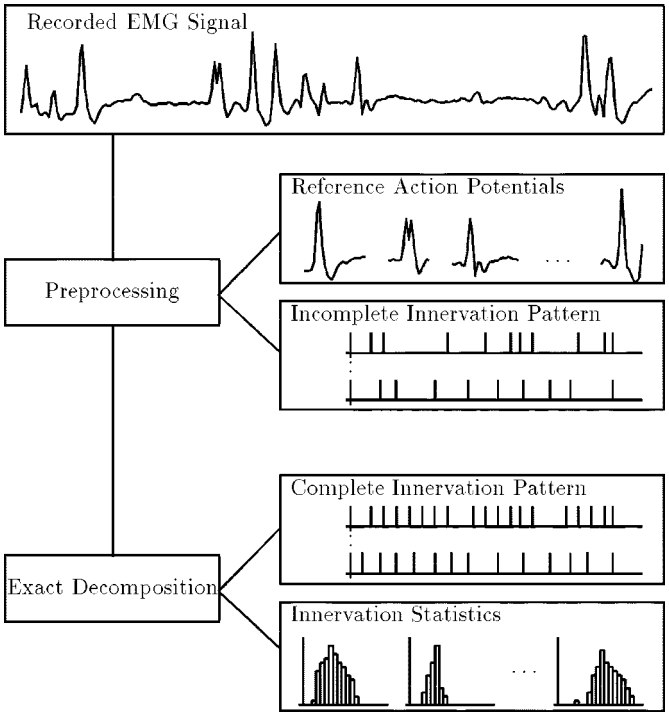

Fig. 1. Required processing steps.

EMG is separated into a number of active segments and in which the unknown waveforms are determined.

The second is the decomposition phase, in which we separate superimposed MUAPs to get the complete innervation pattern.

In this section, we summarize the preprocessing phase developed and implemented by Haas [9] at our Institute, prior to the work reported here. First, the EMG signal is bandpass filtered to remove baseline wander and to shorten the duration of the MUAP's. After filtering, the EMG signal is divided into active and inactive phases. The active phases, containing isolated and superimposed MUAPs, are referred to as *active segments* (AcS). The beginning and end of the AcSs is determined by the activity of the EMG. For the segmentation, a sliding time window is used. If the mean slope within this window exceeds a certain threshold, the beginning of an AcS is postulated. The end of a segment is reached when the total variation of the EMG within the window falls below another threshold. The analysis is restricted to the AcSs, and all decisions in the analysis are made on these data blocks.

After the segmentation, one is left with a number AcSs, which may contain noise, artefacts, a single isolated MUAP, or superimposed MUAP's. The AcSs serve as a basis for the next step, in which one tries to find the waveforms of the individual MUAP's involved in the EMG signal. This is done by a cluster analysis, which is a well-proven tool for the sorting of groups of similar segments. In our case, the fast single linkage algorithm [16] is used (Fig. 2). It consists of the following steps.

- The minimal Euclidean distance d_{ij} between two time aligned AcSs is used as a measure for the distance or dissimilarity between AcSs.
- By means of a single linkage cluster analysis, a hierarchy of partitions is built. The hierarchy starts with a partition in which every active segment forms a cluster by itself. A stepwise fusion of the nearest neighboring clusters ends with a single cluster containing all segments.
- The optimum partition is determined by choosing that partition for which the loss of homogenity as defined by [16] with respect to the next partition is maximal.

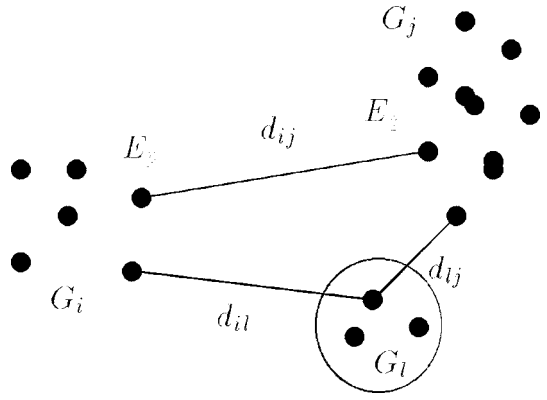

Fig. 2. Single linkage cluster analysis.

The time aligned, filtered, and unfiltered members of each cluster are used to build the corresponding reference action potentials by averaging. For the processing steps that follow, we use the bandpass filtered signal and assume that the MUAPs are time invariant.

III. Mathematical Model

For digital signal processing, the continuous-time EMG signal is digitized at a sampling rate $f_s = 1/T_s = 10$ kHz. The innervation train of MU m is modeled as a point process with firing times n_{mi}. The innervation trains

$$p_m[k] = \sum_{i=0}^{\infty} \delta[k - n_{mi}] \tag{1}$$

represent the innervation of the individual motor units by the central nervous system. The motor unit action potential $s_m[k]$ is modeled as a pulse shaper of finite length

$$s_m[k] = \begin{cases} s_m[k], & 0 \le k \le L \\ 0, & \text{otherwise.} \end{cases} \tag{2}$$

The EMG signal can therefore be written as

$$r[k] = \sum_{l=0}^{L} \sum_{m=1}^{M} p_m[k-l] \cdot s_m[l] + z[k] \tag{3}$$

where M is the number of MUAPs involved in the signal, and $z[k]$ is some kind of additive noise.

At least during constant isometric contraction of the muscle under examination, the interval between two consecutive firings of a MU [the so-called *interpotential interval* (IPI) Δ_{Tm} of the mth MU] may be regarded as a random variable [4] with a unimodal probability density $p_{\Delta_{Tm}(.)}$ with mean m_m and standard deviation σ_m. The mean firing rate $1/m_m$ is typically between 5–25 Hz. The standard deviation σ_m lies between 10–20% of the mean IPI.

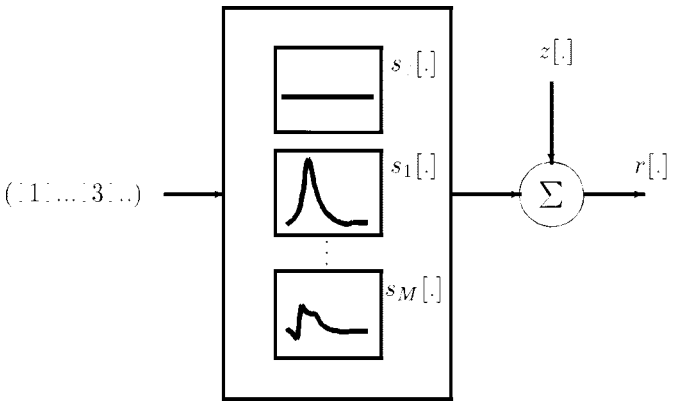

Fig. 3. Model of EMG signal source.

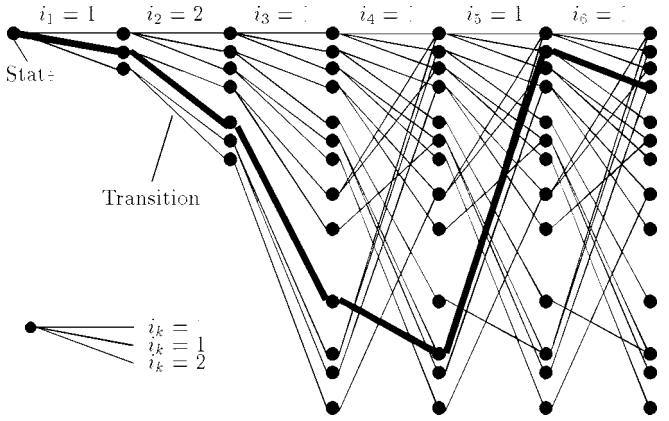

Fig. 4. Trellis of the data source for $M = 2$ and $L = 3$.

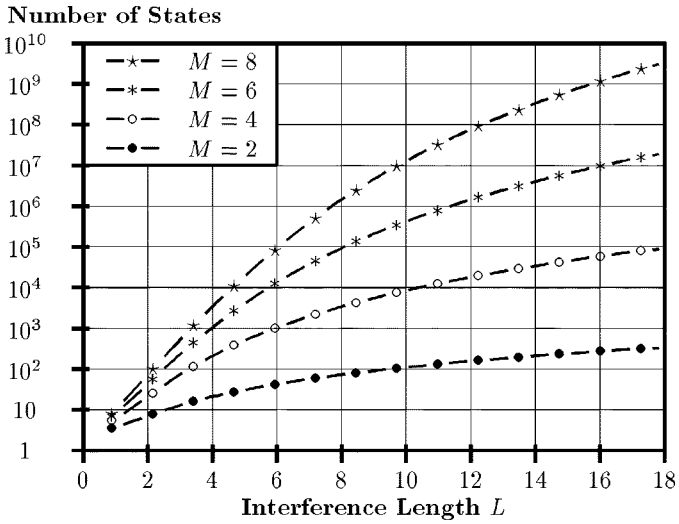

Fig. 5. Number of states N_{Ms} for $M = 2, 4, 6, 8$.

By assuming that in any sampling interval at most one MU becomes active, we can define an innervation sequence $\{i_k\}$

$$\boldsymbol{i}_N = (i_1, i_2, \cdots, i_N) \tag{4}$$

with elements $i_k \in \{0, 1, \cdots, M\}$ to account for the innervation process. An element $i_k \in \{1, \cdots, M\}$ indicates the innervation of the corresponding MU. An element $i_k = 0$ indicates the absence of an innervation. The entire EMG signal can now be described by

$$r[k] = \sum_{l=0}^{L} s_{i_k - l}[l] + z[k] \tag{5}$$

where $s_0[i]$ will be defined as zero for all i. Furthermore, the sequences $\boldsymbol{i}_N$ are constrained in the following way: The same MU m may fire at most once within a window of length $(L+1)$. The justification for this constraint is that the same MU can, for physiological reasons, not be reinnervated during its active time. Due to this property, all sequences violating this restriction are disqualified in our processing scheme.

The resulting system is depicted in Fig. 3 and can be interpreted as an $(M + 1)$-ary digital signaling system with intersymbol interference [17]. The *information* m is conveyed by sending waveform s_m. In spite of the constraint above, $(L+1)$ symbols may overlap causing intersymbol interference. The receiver observes the noisy EMG signal $r[.]$ and has to estimate the information sequence $\boldsymbol{i}_N$, e.g., the sequence $\boldsymbol{i}_N = (0, 1, 0, \cdots, 0, 3, 0, \cdots)$ contained therein. To accomplish this tree-based sequence estimation would, theoretically, be very simple: The set of all information sequences $\boldsymbol{i}_N$ can be drawn as a tree. For each path in the tree, a figure of merit is calculated. The *best* path is assumed to be the best estimate of the innervation sequence. The main drawback of this very simple estimation rule is the computational complexity it involves. For a practical observation length N, the number of paths exceeds what can be computed within reasonable time. Nevertheless, important simplifications can be introduced without any significant loss in quality. Since the EMG source can be modeled as a signaling system with finite intersymbol interference, the encoder shown in Fig. 3 can be thought of as a state machine with a finite number of states. One way of representing such a state machine and its evolution in time is to draw the corresponding trellis diagram (Fig. 4). The trellis diagram represents all possible innervation sequences. Starting from the left in Fig. 4, the innervation sequence $\boldsymbol{i}_N$ decides over the path taken through the trellis. The states are given by the history of the in-going path, the transitions are given by the possible innervations. The example path shown in bold represents the innervation sequence $\boldsymbol{i}_N = (1, 2, 0, 0, 1, 0)$.

The number of states is given by

$$N_{Ms} = \sum_{i=0}^{M} \frac{M!}{(M-i)!} \cdot \frac{L!}{(L-i)! \cdot i!} \tag{6}$$

and shown for various numbers of motor units M in Fig. 5.

Although the introduced restriction reduces the number of states drastically, it is still too large to lead to a reasonable algorithm. To eliminate the least important states, i.e., those states that rarely occur in practice, we introduce the following additional restriction: Within a window of length $(L + 1)$, at most Q elements $(Q < M)$ will be nonzero in $\boldsymbol{i}_N$. Equivalently, we can say that in the sequence of $(Q + 1)$ innervations, no interference occurs between the MUAP starting first and the one starting at the $(Q+1)$th position. It turns out that as long as the EMG signal activity (number of samples in active phases/total number of samples) is less than about 50%, $Q = 2$ still gives excellent results. That a small Q is sufficient reflects the fact

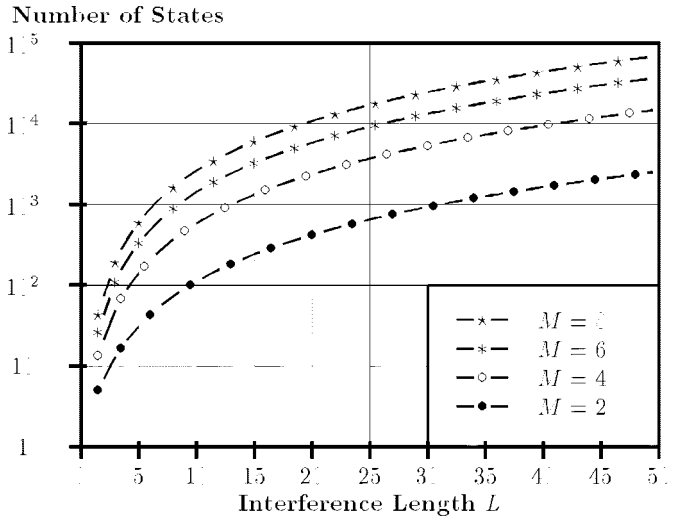

Fig. 6. Number of states $\tilde{N}_{Ms}$ for $M = 2, 4, 6, 8$.

that even in superpositions, only a small number of symbols in $\boldsymbol{i}_N$ are not equal to zero. Sequences fulfilling both mentioned restrictions will later be referred to as *sparse sequences*. With the additional restriction, the number of required states is given by

$$\tilde{N}_{Ms} = \sum_{i=0}^{Q} \frac{M!}{(M-i)!} \cdot \frac{L!}{(L-i)! \cdot i!}. \tag{7}$$

For $Q = 2$, $M = 8$, and $L = 20$, the Viterbi algorithm requires about 10 000 states (Fig. 6).

The next section will show how an optimal sequence estimation can be formulated and how *a priori* knowledge about the sequence $\boldsymbol{i}_N$ can be taken into account.

IV. Decomposition

The model introduced in Section III gives a complete and accurate description of the communication technical equivalent of an observed EMG signal and its underlying innervation process. Given the model of the transmitter (see Fig. 3), we are looking for the optimal receiver, i.e., for the optimal decoder to estimate the innervation sequence $\boldsymbol{i}_N$. The Viterbi algorithm is tailored to calculate the most probable path through the trellis of the encoder in a very efficient way. An in-depth description of the ML sequence estimation using the Viterbi algorithm can be found in [17].

A. Maximum a Posteriori Sequence Estimation

The ML sequence estimation does not use any *a priori* knowledge about the sequence $\boldsymbol{i}_N$. In particular, it does not take into account that the interpotential interval $\Delta_{\mathcal{I}m}$ of the mth MU is a random variable with a unimodal probability density $p_{\Delta_{\mathcal{I}m}}(.)$. Now, the question arises how far the decomposition can be improved by using this knowledge. For the derivation, we start with the MAP decision rule: Choose the sequence $\boldsymbol{i}_N$ that maximizes

$$\begin{aligned} P(\boldsymbol{I}_N = \boldsymbol{i}_N) \cdot p(\boldsymbol{R}_N = \boldsymbol{r}_N | \boldsymbol{I}_N = \boldsymbol{i}_N) \\ = P_{\boldsymbol{I}_N}(\boldsymbol{i}_N) \cdot p_{\boldsymbol{R}_N|\boldsymbol{i}_N}(\boldsymbol{r}_N|\boldsymbol{i}_N) \\ = P(\boldsymbol{i}_N) \cdot p(\boldsymbol{r}_N|\boldsymbol{i}_N) \end{aligned} \tag{8}$$

where $P_{\boldsymbol{i}_N}(\boldsymbol{i}_N)$ denotes the probability of a certain innervation pattern $\boldsymbol{i}_N$, and $p_{\boldsymbol{R}_N|\boldsymbol{I}_N}(\boldsymbol{r}_N|\boldsymbol{i}_N)$ is the conditional probability density of the observation $\boldsymbol{r}_N$ given $\boldsymbol{i}_N$. For readability reasons and as far as possible, the shorter nomenclature $P(\boldsymbol{i}_N)$ and $p(\boldsymbol{r}_N|\boldsymbol{i}_N)$ will be used from this point on.

First of all, it has to be realized that there is no practical way of evaluating (8) for all sparse sequences $\boldsymbol{i}_N$. However, by assuming that the innervation processes of different MU's are statistically independent and that the already-estimated innervations are correct, although some may be missing, a MAP sequence estimation for each AcS can be formulated. To do so, we start by dividing the sequence $\boldsymbol{i}_N$ into three parts:

$$\begin{aligned} \boldsymbol{i}_N &= \{i_1, \cdots, i_a, i_{a+1}, \cdots, i_{a+n}, i_{a+n+1}, \cdots, i_N\} \\ &= \left\{\boldsymbol{i}_{\cdot}^{(1)}, \boldsymbol{i}_n^{(2)}, \boldsymbol{i}_{\cdot}^{(3)}\right\}. \end{aligned} \tag{9}$$

Part $\boldsymbol{i}_{\cdot}^{(1)}$ corresponds to the portion of the EMG that we have already decomposed. $\boldsymbol{i}_n^{(2)}$ stands for the AcS of length n on which our attention is focused, i.e., which we intend to decompose. Part $\boldsymbol{i}_{\cdot}^{(3)}$ represents the remaining AcS with firing time points obtained by the initial cluster analysis. The dots in $\boldsymbol{i}_{\cdot}^{(1)}$ and in $\boldsymbol{i}_{\cdot}^{(3)}$ indicate that the length of these two sequences is not critical. The MAP estimation rule for the AcS corresponding to $\boldsymbol{i}_n^{(2)}$ then reads as follows.

Choose the sequence $\boldsymbol{i}_n^{(2)}$ that maximizes

$$P\left(\boldsymbol{i}_n^{(2)} | \boldsymbol{i}_{\cdot}^{(1)}, \boldsymbol{i}_{\cdot}^{(3)}\right) \cdot p\left(\boldsymbol{r}_n^{(2)} | \boldsymbol{i}_n^{(2)}\right) \tag{10}$$

where $P(\boldsymbol{i}_n^{(2)}|\boldsymbol{i}_{\cdot}^{(1)}, \boldsymbol{i}_{\cdot}^{(3)})$ is the probability of the sequence $\boldsymbol{i}_n^{(2)}$ given $\boldsymbol{i}_{\cdot}^{(1)}$ and $\boldsymbol{i}_{\cdot}^{(3)}$, and $p(\boldsymbol{r}_n^{(2)}|\boldsymbol{i}_n^{(2)})$ stands for the probability density of $\boldsymbol{r}_n^{(2)}$ given $\boldsymbol{i}_n^{(2)}$. The sequence $\boldsymbol{r}_n^{(2)}$ denotes the part of the observation corresponding to $\boldsymbol{i}_n^{(2)}$. If a white noise process is assumed, we can equivalently maximize the product

$$\prod_{k=1}^{n} P\left(i_k^{(2)} | \boldsymbol{i}_{\cdot}^{(1)}, \boldsymbol{i}_{\cdot}^{(3)}\right) \cdot p\left(r_k^{(2)} | i_{k-L}^{(2)}, i_{k-L+1}^{(2)} \cdots, i_k^{(2)}\right). \tag{11}$$

Now, we focus our attention on the *a priori* probability $P(i_k|\boldsymbol{i}_{\cdot}^{(1)}, \boldsymbol{i}_{\cdot}^{(3)})$. According to the underlying model and the assumed mutual independence of the firing patterns, we can write

$$P\left(I_k = m | \boldsymbol{i}_{\cdot}^{(1)}, \boldsymbol{i}_{\cdot}^{(3)}\right) = P(I_k = m | \Delta_l = \delta_l, \Delta_n = \delta_n) \tag{12}$$

where δ_l stands for the number of samples between the current interval k and the last innervation of the mth MU in $\boldsymbol{i}_{\cdot}^{(1)}$, and δ_n stands for the number of samples to the next innervation of the mth MU in $\boldsymbol{i}_{\cdot}^{(3)}$.

By changing the conditioning in (12), different *a priori* knowledge can be introduced in the decomposition. For example, we may assume the following.

- Only the mean m_m of the interpotential intervals are known, i.e., the probabilities $P(I_k = m)$ may be used to improve the decomposition.
- The probability densities $p_{\Delta_{\mathcal{I}m}}(.)$ are given, and the last known innervation of the mth MU was δ_l samples earlier, i.e., the probabilities $P(I_k = m|\Delta_l = \delta_l)$ may be utilized to improve the decomposition.

- The probability densities $p_{\Delta_{\mathcal{T}m}}(.)$ are given, the last known innervation of the m^{th} MU was δ_l samples earlier, and the next known innervation of the same MU takes place in δ_n samples, i.e., the probabilities $P(I_k = m|\Delta_l = \delta_l, \Delta_n = \delta_n)$ may be taken into account to improve the decomposition.

Now, we are left with the problem of determining the probabilities for these three cases. The probability $P(I_k = m)$ is obviously given by

$$P(I_k = m) = P_{I_k}(m) = \frac{T_s}{m_m} \tag{13}$$

where m_m is the known mean IPI, and T_s is the duration of a sampling interval. The derivation of the probability $P(I_k = m|\Delta_l = \delta_l)$ takes a few more steps. Before doing this, however, we have to point out that it is important to consider trains with missing innervations. In practice, not every innervation will be identified. Furthermore, some innervations may really be absent. Unlike McGill [19], we do not wish to make any assumptions about the probability of missing detections. The solution for the probability $P_{I_k|\Delta_l}(m|\delta_l)$, i.e., the probability of an innervation of the mth MU during the interval $\mathcal{K} = \{\mathcal{K} \in R|kT_s \leq \mathcal{K} < (k+1)T_s\}$ given $\mathcal{T}_{m0} = \tau_{m0}$ can be found by resolving the following sum:

$$\begin{aligned}
&P_{I_k|\Delta_l}(m|\delta_l) \\
&\quad = P(I_k = m|\mathcal{T}_{m0} = \tau_{m0}) \\
&\quad = P(\mathcal{T}_{m1} \in \mathcal{K}|\mathcal{T}_{m0} = \tau_{m0}) \\
&\qquad + P(\mathcal{T}_{m1} < kT_s|\mathcal{T}_{m0} = \tau_{m0}) \\
&\qquad \cdot P(\mathcal{T}_{m2} \in \mathcal{K}|\mathcal{T}_{m1} < kT_s, \mathcal{T}_{m0} = \tau_{m0}) \\
&\qquad + P(\mathcal{T}_{m1} < kT_s|\mathcal{T}_{m0} = \tau_{m0}) \\
&\qquad \cdot P(\mathcal{T}_{m2} < kT_s|\mathcal{T}_{m1} < kT_s, \mathcal{T}_{m0} = \tau_{m0}) \\
&\qquad \cdot P(\mathcal{T}_{m3} \in \mathcal{K}|\mathcal{T}_{m1} < kT_s, \mathcal{T}_{m2} < kT_s, \mathcal{T}_{m0} = \tau_{m0}) \\
&\qquad + \cdots \\
&\quad = \sum_{i=1}^{\infty} P(\underbrace{\mathcal{T}_{mi} \in \mathcal{K}}_{\text{Event } \mathcal{A}}, \underbrace{\bigcap_{j=0}^{i-1} \mathcal{T}_{mj} < kT_s}_{\text{Event } \mathcal{B}} |\mathcal{T}_{m0} = \tau_{m0}) \\
&\quad = P(\underbrace{\mathcal{T}_{mi} \in \mathcal{K}}_{\text{Event } \mathcal{A}}|\mathcal{T}_{m0} = \tau_{m0})
\end{aligned} \tag{14}$$

where $\mathcal{T}_{mi}$ is a random variable defined by

$$\mathcal{T}_{mi} = \mathcal{T}_{m0} + \sum_{k=1}^{i} \Delta_{mk}.$$

Δ_{mi} is the random quantity describing the IPI in the mth innervation train, and $\mathcal{T}_{m0}$ is the time point of the 0th innervation. Since $\Delta_{mi} > 0$ holds for any i, we can deduce that event $\mathcal{B}$ always occurs when event $\mathcal{A}$ is true. The probability $P_{I_k|\Delta_l}(m|\delta_l)$ is therefore given by

$$\begin{aligned}
P_{I_k|\Delta_l}(m|\delta_l) &= \sum_{i=1}^{\infty} P(\mathcal{T}_{mi} \in \mathcal{K}|\mathcal{T}_{m0} = \tau_{m0}) \\
&= \sum_{i=1}^{\infty} \int_{\delta_l T_s}^{(\delta_l+1)T_s} p^{(i)}_{\Delta_{\mathcal{T}m}}(\tau)\, d\tau
\end{aligned}$$

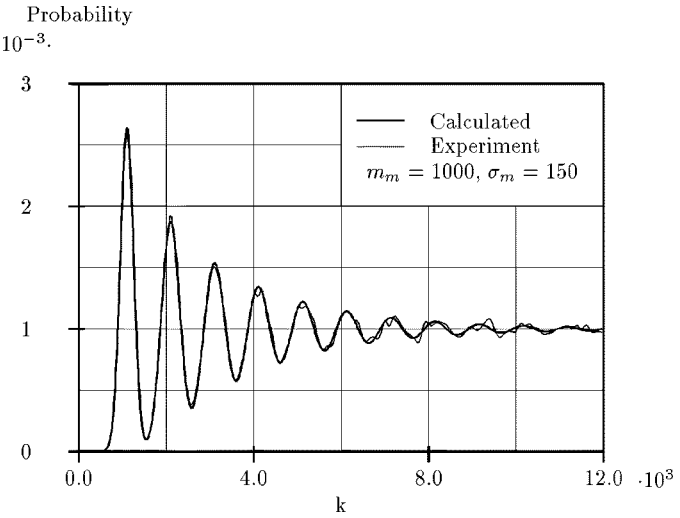

Fig. 7. Probability of an innervation in the kth sampling interval given an innervation in the 0th interval. The mean IPI is assumed to be $1000 \cdot T_s$ with a standard deviation of $150 \cdot T_s$.

where

$$p^{(i)}_{\Delta_{\mathcal{T}m}}(.) = \begin{cases} p_{\Delta_{\mathcal{T}m}}(.), & \text{for } i = 1 \\ p^{(i-1)}_{\Delta_{\mathcal{T}m}}(.) * p_{\Delta_{\mathcal{T}m}}(.), & \text{for } i \geq 2 \end{cases}$$

arises from continued convolution of $p_{\Delta_{\mathcal{T}m}}(.)$. An example of $P_{I_k|\Delta_l}(m|\delta_l)$ for a Gaussian probability density $p_{\Delta_{\mathcal{T}m}}(.)$ is shown in Fig. 7.

Given the solution for $P_{I_k|\Delta_l}(m|\delta_l)$, the probability $P(I_k = m|\Delta_l = \delta_l, \Delta_n = \delta_n)$, i.e., the probability of an innervation of MU m within interval k for a given $\Delta_l = \delta_l$ and $\Delta_n = \delta_n$, can now easily be derived:

$$\begin{aligned}
&P(I_k = m|\Delta_l = \delta_l, \Delta_n = \delta_n) \\
&\quad = P_{I_k|\Delta_l, \Delta_n}(m|\delta_l, \delta_n) \\
&\quad = \frac{P(I_k = m, \Delta_n = \delta_n|\Delta_l = \delta_l)}{P(\Delta_n = \delta_n|\Delta_l = \delta_l)} \\
&\quad = \frac{P(I_k = m|\Delta_l = \delta_l) \cdot P(\Delta_n = \delta_n|\Delta_l = \delta_l, I_k = m)}{P(\Delta_n = \delta_n|\Delta_l = \delta_l)}.
\end{aligned} \tag{15}$$

By using the fact that

$$P(\Delta_n = \delta_n|\Delta_l = \delta_l, I_k = m) = P(\Delta_n = \delta_n|I_k = m)$$

we finally obtain

$$\begin{aligned}
&P_{I_k|\Delta_l, \Delta_n}(m|\delta_l, \delta_n) \\
&\quad = \frac{P(I_k = m|\Delta_l = \delta_l) \cdot P(\Delta_n = \delta_n|I_k = m)}{P(\Delta_n = \delta_n|\Delta_l = \delta_l)}.
\end{aligned} \tag{16}$$

Fig. 8 shows an example of $P_{I_k|\Delta_l, \Delta_n}(m|\delta_l, \delta_n)$ for a Gaussian probability density $p_{\Delta_{\mathcal{T}m}}(.)$.

The last two functions are worth examining in more detail. To our satisfaction they exhibit the following behavior:

- The function $P_{I_k|\Delta_l}(m|\delta_l)$ tends toward $P_{I_k}(m) = T_s/m_m$ for $k \to \infty$.
- The function $P_{I_k|\Delta_l, \Delta_n}(m|\delta_l, \delta_n)$ tends toward $P_{I_k|\Delta_l}(m|\delta_l)$ for $\delta_n \to \infty$.

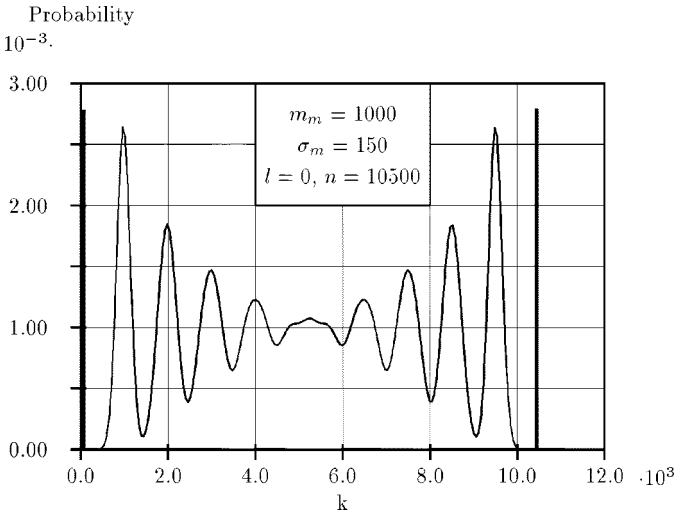

Fig. 8. Probability of an innervation in the kth sampling interval given innervations at 0 and 10 500. The mean IPI is again assumed to be $1000 \cdot T_s$ with a standard deviation of $150 \cdot T_s$.

This is due to the fact that the larger the distance to a known innervation, the smaller the information carried by the corresponding condition.

Until now, we have not restricted ourselves to any special probability density $p_{\Delta_{Tm}}(.)$. After a closer look at a typical interpotential interval histogram, it seems reasonable to use a Gaussian distribution, as suggested by McGill [19], i.e., we choose

$$p_{\Delta_{Tm}}(t) = \frac{1}{\sqrt{2 \cdot \pi}\sigma_m} e^{-((t-m_m)^2/2 \cdot \sigma_m^2)}. \tag{17}$$

By doing so, $p^{(i)}_{\Delta_{Tm}}(.)$ is given by

$$p^{(i)}_{\Delta_{Tm}}(t) = \frac{1}{\sqrt{2 \cdot \pi \cdot i}\sigma_m} e^{-((t-i \cdot m_m)^2/2 \cdot i \cdot \sigma_m^2)} \tag{18}$$

so that $P_{I_k|\Delta_l}(m|\delta_l)$ and $P_{I_k|\Delta_l,\,\Delta_n}(m|\delta_l,\,\delta_n)$ can be easily calculated. The mean m_m and the standard deviation σ_m need to be estimated from the initial cluster analysis.

Putting these facts together, we are now able to maximize (10) by using the Viterbi algorithm [18], as described in [15] for the ML case. The Viterbi algorithm can be thought of as an algorithm with the same states and transitions as the corresponding encoder. It calculates the most probable path through the trellis by calculating a figure of merit (the so-called *metric* for a certain path in the trellis recursively). For the metric $\mu_1(\boldsymbol{i}^{(2)}_{L+1})$, we get

$$\begin{aligned}\mu_1(\boldsymbol{i}^{(2)}_{L+1}) &= \mu_1(i^{(2)}_1, i^{(2)}_2, \cdots, i^{(2)}_{L+1}) \\ &= \mu_1(i_{a+1}, i_{a+2}, \cdots, i_{a+L+1}) \\ &= \max_{i_{a+1}} \left(\sum_{k=a+1}^{a+L+1} \ln(P(i_k|.) \right. \\ &\qquad \left. \cdot p(r[k]|i_{k-L}, i_{k-L+1}, \cdots, i_k) \right) \end{aligned} \tag{19}$$

and in general, $\mu_k(\boldsymbol{I}_{L+k})$ is obtained by

$$\begin{aligned}&\mu_k(\boldsymbol{i}^{(2)}_{L+k}) \\ &\quad = \max_{i_{a+k}} \Big(\ln(p(r[a+L+k]|i_{a+k}, i_{a+k+1}, \cdots, i_{a+L+k}) \\ &\qquad \cdot P(i_{a+L+k}|.)) + \mu_{k-1}\left(\boldsymbol{i}^{(2)}_{L+k-1}\right)\Big) \\ &\quad = \max_{i_{a+k}} \Big(\ln(p(r[a+L+k]|\tilde{r}[a+L+k]) \cdot P(i_{a+L+k}|.)) \\ &\qquad + \mu_{k-1}\left(\boldsymbol{i}^{(2)}_{L+k-1}\right)\Big), \\ &\quad = \max_{i_{a+k}} \Big(-|r[a+L+k] - \tilde{r}[a+L+k]| \\ &\qquad + \frac{\sigma_Z}{\sqrt{2}} \cdot \ln(P(i_{a+L+k}|.)) + \mu_{k-1}\left(\boldsymbol{i}^{(2)}_{L+k-1}\right)\Big) \end{aligned} \tag{20}$$

where $\tilde{r}[a+L+k]$ is the noiseless EMG signal for the given path through the encoder

$$\tilde{r}[a+L+k] = \sum_{l=0}^{L} s_{i_{a+L+k-l}}[l]$$

and σ_Z stands for the noise standard deviation. Furthermore, a common constant term in (20) is dropped, and a Laplacian noise probability density is assumed. This assumption showed in all the decompositions carried out at our laboratory a slightly higher detection rate. For $P(I_k|.)$, any of the three derived probabilities can be used.

In contrast with the metric given in the ML case, the derived metric requires an estimation of the noise variance. In addition, we note that choosing $\sigma = 0$ brings us back to the ML decision criterion.

V. Results

The proposed algorithms were implemented and tested both with clinically measured and with artificially generated EMG signals. The segmentation and the MUAPs were obtained with our standard analysis package ARTMUP [9]. After filtering, the decomposition was carried out at a sampling rate of 5 kHz and a fixed MUAP length of 4.2 ms, i.e., 21 samples. We compared the obtained firing patterns with those obtained by laborious manual decomposition. Two different kinds of quality criteria were used:

- percentage of correctly detected innervations;
- percentage of false alarms, i.e., detections in intervals with no innervation.

To provide more information about the analyzed signals, the following additional characteristic data relating to the measured EMG signal are given in Table I:

- EMG activity as given by (3);
- number of MUAPs;
- mean firing rate;
- standard deviation of the additive noise term.

All EMG signals were normalized to $\max|r[k]| = 1.0$

The measured EMG signals were taken from the muscle biceps, and the recording was done at a sampling rate of 10 kHz.

TABLE I
CHARACTERISTIC DATA OF ANALYZED EMG SIGNALS

EMG signal	Signal activity	Number of MUAP's	Mean firing rate	σ_Z
1	48%	5	11 Hz	0.038
2	51%	6	10 Hz	0.040
3	19%	4	12 Hz	0.046
4	59%	5	16 Hz	0.057
5	27%	4	14 Hz	0.035
6	41%	4	10 Hz	0.048
7	48%	7	13 Hz	0.040
8	41%	5	9 Hz	0.047
9	41%	5	10 Hz	0.046
10	44%	7	8 Hz	0.043
Mean	42%	5	11 Hz	0.044
Std	11.5%	1	2.5 Hz	0.062

TABLE II
ACHIEVED DECOMPOSITION ACCURACY WITH MEASURED EMG SIGNALS, i.e., PERCENTAGE OF CORRECTLY DETECTED AND ADDITIONALLY ESTIMATED INNERVATIONS

EMG signal	ML estimation		MAP estimation	
1	91.1%	8.3%	94.4%	4.5%
2	90.3%	5.9%	91.9%	4.0%
3	95.5%	13.2%	95.0%	7.3%
4	88.0%	8.4%	91.0%	5.6%
5	95.9%	4.3%	95.4%	0.8%
6	94.0%	2.6%	95.7%	2.3%
7	86.9%	13.8%	91.6%	5.3%
8	93.2%	4.5%	95.2%	2.1%
9	92.0%	4.4%	93.4%	2.5%
10	98.4%	2.6%	98.6%	0.8%
Mean	92.5%	6.8%	94.2%	3.5%
Std	3.6 %	4.0%	2.3%	2.2%
Total error	**14.3%**		**9.3%**	

The analysis was carried out after filtering and down sampling the signal to 5 kHz. In Table II, the results for the ten measured EMG signals are given.

To eliminate the uncertainty of the manual decompositions, a corresponding set of ten artificially generated EMG signals was produced. The artificial EMG signals were based on the manual decomposition. Two different cases were studied: the decomposition of a noiseless set of EMG signals and the decomposition of EMG signals with the same noise floor as the original signals. Table III summarizes the results obtained for both cases. The decomposition was carried out with the described MAP sequence estimation.

The test of the implemented estimation algorithms proves the validity of the introduced concept: The analysis of ten measured EMG signals leads in the mean to 92.5% correctly detected and 6.8% additionally estimated innervations in the ML case. With the MAP sequence estimation, we obtain in the mean 94.2% correctly detected and 3.5% additionally estimated innervations and thereby improved the total accuracy by 5% over the ML case.

The decomposition of the artificially generated EMG signals leads to the following conclusion. Since the decomposition of noiseless signals results in about 3% errors, we have to deduce that they arise from our definition of sparseness.

TABLE III
ACHIEVED DECOMPOSITION ACCURACY WITH ARTIFICIALLY GENERATED EMG SIGNALS, i.e., PERCENTAGE OF CORRECTLY DETECTED AND ADDITIONALLY ESTIMATED INNERVATIONS

EMG signal	Noiseless EMG MAP estimation		Equivalent EMG MAP estimation	
1	96.7%	1.4%	95.7%	1.3%
2	96.2%	0.7%	94.7%	1.9%
3	98.6%	0.0%	94.5%	5.9%
4	96.4%	0.6%	92.9%	1.9%
5	98.7%	0.0%	97.2%	1.3%
6	98.0%	0.3%	97.4%	0.7%
7	96.9%	0.9%	96.3%	1.0%
8	98.3%	0.7%	94.9%	4.1%
9	96.4%	0.8%	94.7%	2.5%
10	99.4%	0.0%	99.2%	0.4%
Mean	97.6%	0.5%	95.8%	2.1%
Std	1.2 %	0.5%	1.8%	1.7%
Total error	**2.9%**		**6.3%**	

Between the results obtained for the artificial EMG signals with noise and the one for the measured signals is again a gap of about 3%. This difference comes from rarely occurring MUAPs not covered by the used set of MUAPs and from faults in the manual decomposition.

Therefore, we can conclude that about 3% of the errors are caused by the restriction of the innervation sequence. Further, 3% are created by the additive noise term. The last 3% stem from faults in the manual decomposition and rarely occurring MUAPs.

VI. CONCLUSION

In this paper, a new EMG signal decomposition approach is introduced. It is shown that the EMG signal source can be modeled as a $(M+1)$-ary signaling system with intersymbol interference. The corresponding encoder would lead to a state machine with about $\approx 10^{10}$ states. Due to the special nature of the EMG signal, a concept of sparse sequences can be applied. The resulting encoder requires only on the order of 10^4 states. In accordance with communication technical concepts, a MAP sequence estimation based on the Viterbi algorithm is formulated.

In retrospect, it seams reasonable to analyze the communication between neurons and muscles by communication technical means. This point of view allows a very clear understanding of the problem under consideration. Nevertheless, only the concept of sparse sequences makes the algorithm practical.

The algorithms introduced are tailored for accurate EMG signal decomposition. They demonstrate the difference in accuracy that can be obtained by introducing *a priori* knowledge about the innervation statistics. The algorithms are implemented on a signal processor board from AT&T. The analysis of 10 s of EMG signal takes between 2 and 3 min.

REFERENCES

[1] J. J. Kelly, Jr., *Electromyography for the Clinician in Clinical Medicine*, J. A. Spittel Jr., Ed. Philadelphia, PA: Harper-Row, 1981.
[2] J. Kimura, *Electrodiagnosis in Diseases of Nerve and Muscle: Principles and Practice*. Philadelphia, PA: F. A. Davis, 1983.
[3] F. Buchthal, "Electromyography in the evaluation of muscle diseases," *Neurolog. Clinics*, vol. 3, pp. 573–598, 1985.

[4] R. S. LeFever, "Statistical analysis of concurrently active human motor units," Ph.D. dissertation, Mass. Inst. Technol., Cambridge, Feb. 1980.
[5] R. S. LeFever and C. J. De Luca, "A procedure for decomposing the myoelectric signal into its constituent action potentials," *IEEE Trans. Biomed. Eng.*, vol. BME-29, pp. 149–153; 158–164, Mar. 1982.
[6] R. G. Lee and D. G. White, "Computer analysis of motor unit action potentials in routine clinical electromyograpyh," in *New Developments in Electromyography and Clin. Neurophysiology*, J. E. Desmedt, Ed. Basel, Switzerland: Karger, 1973, pp. 454–461.
[7] A. Gerber, R. M. Studer, R. J. P. de Figueiredo, and G. S. Moschytz, "A new framework and computer program for quantitative EMG signal analysis," *IEEE Trans. Biomed. Eng.*, vol. BME-31, pp. 857–863, Dec. 1984.
[8] R. M. Studer, R. J. P. de Figueiredo, and G. S. Moschytz, "An algorithm for sequential signal estimation and system identification for EMG signals," *IEEE Trans. Biomed. Eng.*, vol. BME-31, pp. 285–295, Mar. 1984.
[9] W. F. Haas and M. Meyer, "An automatic EMG decomposition system for routine clinical examination and clinical research," in *Computer-Aided Electromyography and Expert Systems*. Amsterdam, The Netherlands: Elsevier, 1989.
[10] M. H. Hassoun, C. Wang, and A. R. Spitzer, "NNERVE: Neural network extraction of repetitive vectors for elektromyography," *IEEE Trans. Biomed. Eng.*, vol. 41, p. 1039–1061, Nov. 1994.
[11] B. Mambrito and C. De Luca, "Acquisition and decomposition of the EMG signal," in *Computer-Aided Electromyography, Prog. in Clin. Neurophysiology*, J. E. Desmedt, Ed. Basel, Switzerland: Karger, 1983, vol. 10.
[12] R. Gut, P. Kreier, and G. S. Moschytz, "Trellis-based deconvolution of ultrasonic echoes," in *Proc. IEEE Int. Symp. Circuits Syst.*, vol. 2, Seattle, WA, May 1995, pp. 1384–1387.
[13] J. A. Jensen and J. Mathorne, "Deconvolution of in-vivo ultrasound B-mode images," *Ultrason. Imag.*, vol. 15, pp. 122–133, Apr. 1993.
[14] M. Hufschmid, "Maximum-likelihood processing of signals received over multipath channels," Ph.D. dissertation, ETH, Zürich, Switzerland, 1992.
[15] R. Gut and G. S. Moschytz, "High-precision EMG signal decomposition with modified Viterbi algorithm," in *Proc. IEEE Int. Symp. Circuits Syst.*, vol. 1, Singapore, June 1991, pp. 730–733.
[16] H. Späht, *Cluster Analyze Algorithmen zur Objektklassifizierung und Datenreduktion*. Berlin, Germany: Oldenburg, 1975.
[17] J. G. Proakis, *Digital Communications*. Singapore: McGraw-Hill, 1983.
[18] A. J. Viterbi, "Error bounds for convolutional codes and an asymptotically optimum decoding algorithm," *IEEE Trans. Inform. Theory*, vol. IT-13, pp. 260–269, Apr. 1967.
[19] K. C. McGill and L. J. Dorfman, "Automatic decomposition electromyography (ADEMG). Methodologic and technical considerations," in *Computer-Aided Electromyography and Expert Systems*. Amsterdam, The Netherlands: Elsevier, 1989, pp. 91–101.

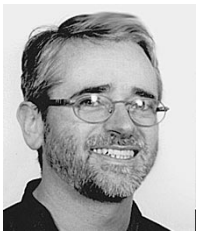

Richard Gut (M'93) was born in Pfäffikon, Switzerland, in 1958. He received the B.E.E. degree from the University of Applied Sciences, Winterthur, Switzerland, in 1981 and the E.E. Diploma and Ph.D. degree from the Swiss Federal Institute of Technology (ETH), Zurich, in 1985 and 1992, respectively.

From 1995 to 1996, he was with AT&T Bell Laboratories, Middletown, NJ, where he was working in the field of digital communication. From 1997 to 1999, he was with the spin-off company Globespan, Red Bank, NJ, where he was leading a software group developing code for high-speed DSL modems. Since 1999, he has been a Professor at the University of Applied Sciences, Muttenz, Switzerland. His interests are mainly in the fields of signal processing, estimation theory, and digital communication.

George S. Moschytz (M'65–SM'77–F'78) received the E.E. Diploma and the Ph.D. degree from the Swiss Federal Institute of Technology (ETHZ), Zurich, in 1958 and 1962, respectively.

From 1960 to 1962, he was with RCA Laboratories, Zurich. From 1963 to 1972, he was with Bell Laboratories, Homdel, NJ, where he developed and later supervised methods of designing hybrid-integrated active RC filters and silicon-integrated logic circuits. Since 1973, he has been a Professor of network theory and signal processing and Director of the Signal and Information Processing Laboratory at ETHZ. He has authored and co-authored more than 250 papers in the field of network theory, active and switched-capacitor filter and network design, and sensitivity theory, holds several patents, and is author and co-author of five books in these and related areas. His present interests are analog, digital, switched-capacitor, switched-current, and adaptive filters, cellular neural networks and wavelets for signal processing, and the application of signal processing techniques to medical problems and biosignals.

Prof. Moschytz is President of the IEEE Swiss Chapter on Digital Communication Systems and a Member of the Swiss Electrotechnical Society. From 1981 to 1982, he was President of the Swiss Section of the IEEE. He has had several terms in the Adcom of the IEEE Circuits and Systems Society as well as on the Editorial Board of the PROCEEDINGS OF THE IEEE. He was Associate Editor of the IEEE CIRCUITS AND SYSTEMS MAGAZINE. He is on the Board of Governors of the IEEE Circuits and Systems Society and was President of the Society in 1999. He is an elected member of the Swiss Academy of Engineering Sciences, winner of the Best Paper Award (for a paper on active filter design using tantalum thin-film technology), winner of the IEEE CAS Education Award, and a is member of Eta Kappa Nu.